GEOPHYSICAL RESEARCH LETTERS, VOL. 19, NO. 1, PAGES 1-4, JANUARY 3, 1992

TRAVEL-TIME TOMOGRAPHY IN THE NORTHERN COACHELLA VALLEY USING AFTERSHOCKS OF THE 1986 M_L 5.9 NORTH PALM SPRINGS EARTHQUAKE

Craig Nicholson
Institute for Crustal Studies, University of California at Santa Barbara

Jonathan M. Lees
Department of Geology and Geophysics, Yale University

Abstract. Tomographic inversion is applied to delay times from aftershocks of the 1986 M_L 5.9 North Palm Springs (NPS) earthquake to image 3-D velocity variations within the northern Coachella Valley. P-wave arrival times from 1074 earthquakes, with depths ranging from 3 to 20 km, were used as sources recorded by 12 portable and 4 permanent stations. Preliminary results show well-defined high- and low-velocity anomalies (2–7%) that correlate with the rupture distribution of the 1986 mainshock. At depths less than 8 km, a low-velocity anomaly predominates between the two NE-dipping Banning and Mission Creek faults. From 8 to 12 km in depth, where the NPS mainshock and most of the aftershocks occur, a high-velocity anomaly is observed. This high-velocity feature is interpreted as imaging the asperity responsible for the 1986 rupture; and suggests that velocity information may help to define important elements, such as asperities, that control fault rupture, and thus, may help to predict the location and size of future events.

INTRODUCTION

The M_L 5.9 North Palm Springs earthquake occurred on 8 July 1986; its epicenter (34°00.3'N, 116°36.3'W) was located between the Banning and Mission Creek strands of the southern San Andreas fault (SAF) (Figure 1). The focal depth of the earthquake was between 10 to 11 km. Although the initial rupture was pure strike-slip [*Jones et al.*, 1986], analysis of regional and teleseismic body-waves indicate that the mainshock accommodated up to 0.8 m of right-oblique reverse-slip on the Banning fault with an average dip to the NE of 40°–50° and an average strike between N60°–77°W [*e.g., Hartzell,* 1989]. Seismic moment estimates range from 0.9 to 1.7×10^{18} N-m, with the area of rupture extending roughly 15–22 km along strike and 11–15 km down-dip. Based on the distribution of aftershocks and modelling the slip history of the mainshock, the earthquake is believed to have propagated bilaterally, as well as up- and down-dip, with dynamic slip largely confined between depths of 5 and 13 km (Figure 1).

Following the mainshock, four digital and 8 analog portable seismographs were deployed to record aftershock activity. These instruments supplemented a regional network of permanent stations operated by Caltech and the USGS. The portable stations occupied 17 sites during the period July 9 to July 22 (Figure 2a) and recorded well over 2,000 aftershocks. In this preliminary study of the local 3-D velocity structure in the northern Coachella Valley, we have applied linear tomographic inversion to a subset of 1,074 of these events.

DATA AND DATA ANALYSIS

The data used were selected NPS aftershocks recorded between 8 and 12 July 1986. Hypocenters were first located relative to a 1-D velocity model (Table 1) derived from local seismic refraction work [*Green,* 1983] and analysis of regional earthquake arrival times [*Jones et al.,* 1986]; and then relocated using a set of average station corrections derived from travel-time residuals produced by the previous locations. The earthquakes were located using the computer program HYPOELLISPE [*Lahr,* 1989]. To insure that events with poor locations did not adversely affect the tomographic results, events with fewer than 8 station readings, RMS residuals >0.30 s,

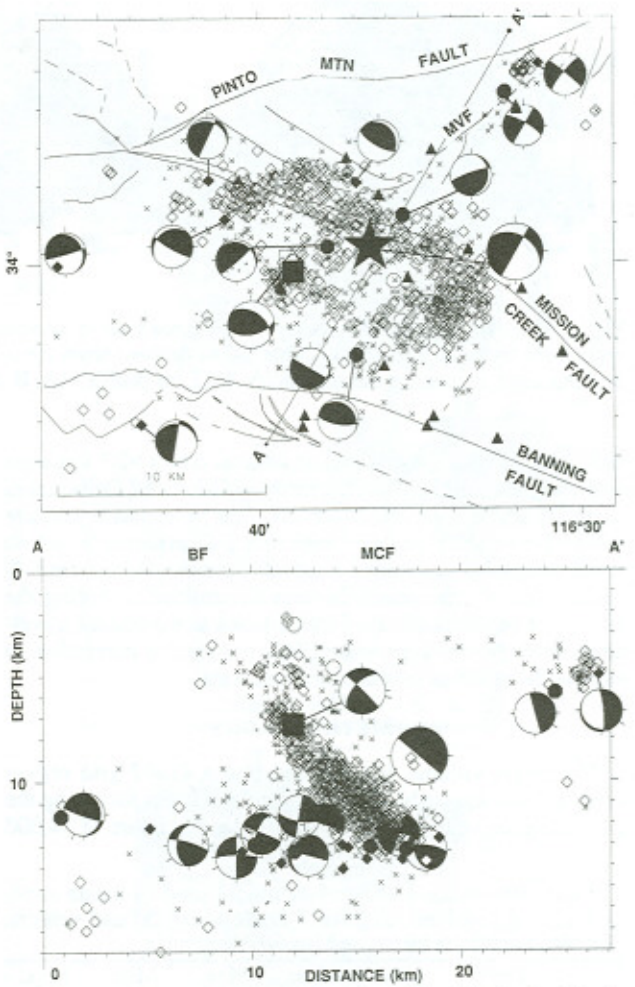

Fig. 1. Map and vertical cross section (A–A') of aftershocks associated with the 1986 NPS earthquake (star); Quaternary faults (solid lines, dashed where buried) are mapped by *Matti et al.* [1985]. Aftershocks define a nearly planar zone dipping about 50°NE. Additional aftershocks occur at shallow depths (< 7 km) to the NE along the Morongo Valley fault (MVF) and at depths >10 km to the SW of the mainshock rupture. Lower-hemisphere and front-projection focal mechanisms of selected deep earthquakes (solid symbols in cross section) exhibit a low-angle nodal plane and suggest seismic slip on a possible NE-dipping detachment. Triangles are stations.

Paper number 91GL03037
0094-8534/92/91GL-03037$03.00

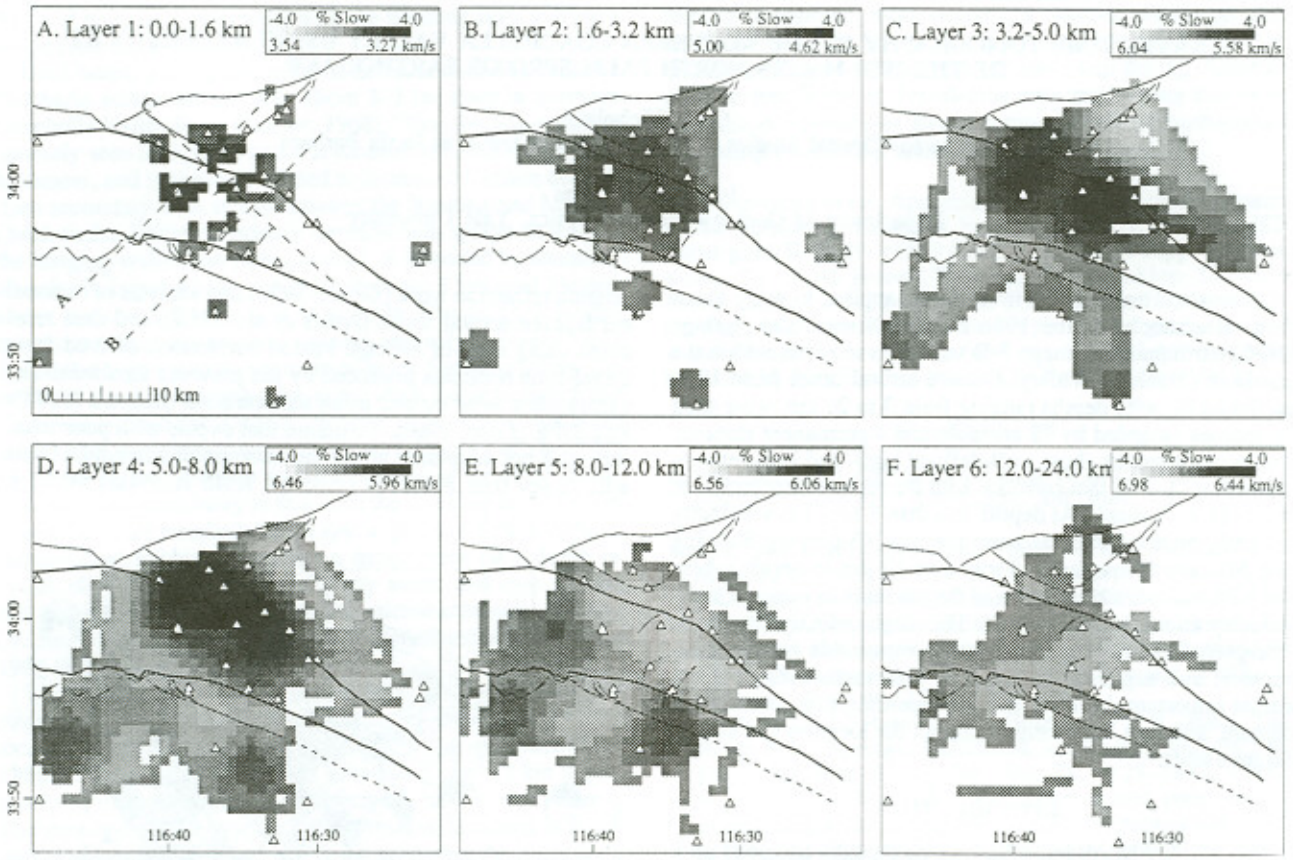

Fig. 2. Grayshade plots of velocity perturbations (in % slowness) relative to homogeneous layer velocities specified in the 1-D model for layers 1 through 6 (Table 1), as derived from the 3-D tomographic inversion. Triangles are portable and permanent stations used to monitor the seismicity. (a) Line profiles (A, B, and C) reflect cross section orientations shown in Figure 4.

and either standard horizontal or vertical errors >2.7 km were excluded, leaving 1,074 sufficiently well-located earthquakes to use as sources for the inversion. The inversion procedure solved for velocity perturbations in a 3-D structure based on initial calculated travel-time residuals determined from the 1-D model. Travel-time residuals were determined by taking the difference between observed travel-times and predicted travel-times through the 1-D model, less the station correction to remove the effect of near receiver structure.

METHODOLOGY

The target volume was divided into a 42×42 grid region using 1.0-km square blocks of varying thickness following the 1-D reference velocity model, yielding a maximum of 14,000 model parameters. Rays were traced through the 1-D model and perturbations of slowness along each ray path were calculated within each block such that the sum of the squared travel-time residuals (observed minus predicted) is minimized. The data were weighted according to estimates of the original quality factors (0–3) provided with each phase reading. Effects of noisy data were reduced by constraining the Laplacian (second spatial derivative) of the slowness field to be zero within horizontal layers, effectively smoothing the model laterally. The resulting system of simultaneous equations was solved by an iterative conjugate gradient technique (LSQR) [*Lees and Crosson,* 1989]. After 30 iterations, the data variance was reduced by 24%. The reduction in data variance was relatively small largely because the observed travel-times were well modeled by the initial 1-D velocity model of homogeneous layers and the applied station corrections.

Table 1. Reference 1-D velocity model used to locate earthquakes and resolved range of 3-D slowness (s) and velocity perturbations from tomographic inversion.

Layer	Depth to top (km)	Ref. vel. (km/s)	Min. % s	Max. % s	Min. vel. (km/s)	Max. vel. (km/s)
1	0.0	3.4	-0.0	+2.1	3.35	3.40
2	1.6	4.8	-0.4	+3.0	4.65	4.80
3	3.2	5.8	-3.3	+4.7	5.55	6.00
4	5.0	6.2	-1.6	+6.7	5.80	6.30
5	8.0	6.3	-2.3	+2.0	6.15	6.45
6	12.0	6.7	-1.2	+0.6	6.65	6.80
7	24.0	6.8	-0.6	+0.2	6.80	6.85
8	32.0	7.8	-0.4	+0.1	7.80	7.85

The influence of data variability on the model was estimated by Jackknife error analysis [*Lees and Crosson,* 1989]. The standard errors (1 σ) calculated in this manner were found to be typically 1% or less (slowness perturbation) over most of the model (Figure 3), suggesting that slowness variations greater than a few percent are significant. Spatial resolution was estimated by calculating impulse responses for different parts of the model [*Lees and Crosson,* 1989]. Near the center of the model, where the ray coverage is most dense, the lateral resolution length was found to be slightly better than 4 km (3–4 blocks) (Figure 3c). The resolution kernels, however, are typically not symmetric due to heterogeneity of ray coverage, and tend to be elongate in a direction perpendicular to the local strike of the SAF. In the vertical direction, smearing due to ray distribution produces point spread functions that are down by

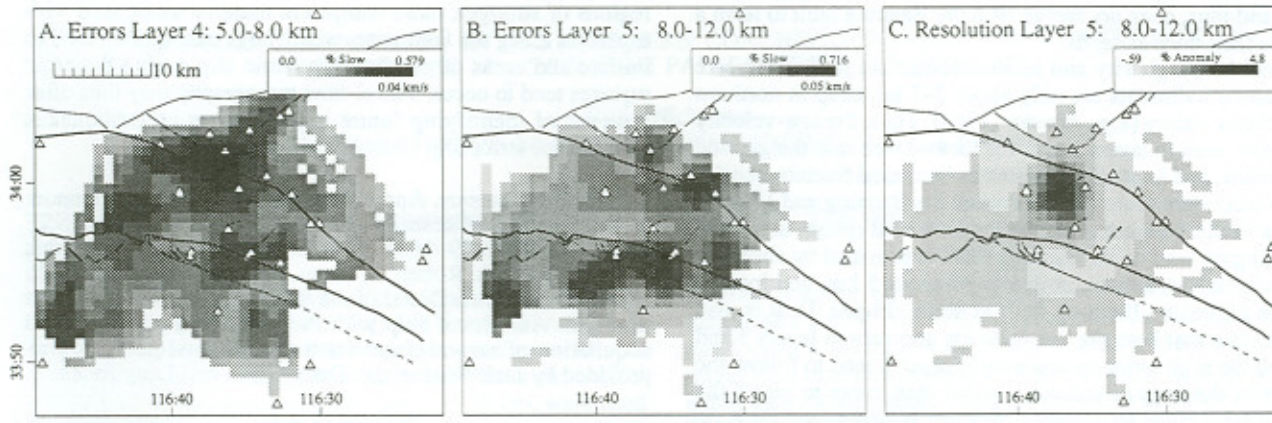

Fig. 3. (a and b) Jackknife error estimates in % slowness perturbation calculated for layers 4 and 5. Minimum error resolution is greatest perpendicular to the major faults and is typically about 1%. (c) Impulse response for a unit velocity perturbation located at the hypocenter of the 1986 mainshock as resolved in layer 5, indicating a lateral resolution near the mainshock of about 3–4 km.

only a third or less of the central point of the resolution kernal. This indicates that the vertical resolution near the NPS mainshock is less than one layer.

Results

The inversion results are displayed as fixed grayshade plots for layers 1–6 (Figure 2) and for several cross sections (Figure 4). The true limits of the slowness perturbation, however, vary from layer to layer (Table 1). By displaying the results as slowness perturbations from the reference 1-D model, the average regional velocity structure, which would otherwise dominate the image, is removed. The top two layers of the 3-D perturbation model have poor lateral resolution because the emerging near-vertical rays are concentrated near the receiving stations. The perturbations observed in these layers range from -1 to +1% and can be simply viewed as minor additions to the station corrections removed prior to the inversion.

Between 3.2–8.0 km depth (Figure 2), there is a prominent low-velocity anomaly (high slowness) located between the Banning and Mission Creek faults directly above the rupture zone of the 1986 NPS earthquake. In 3-D, this low-velocity anomaly is clearly bounded on the SW by the NE-dipping Banning fault (Figure 4). By layer 5 (8.0–12.0 km depth), the large low-velocity anomaly between the Banning and Mission Creek faults seen in layers 3 and 4 has changed into a high-velocity anomaly. Nearly all the aftershocks and nearly all the dynamic slip observed during the 1986 mainshock (C–C', Figure 4) occurred within layer 5 and within the area defined by the high-velocity perturbation. Below 12.0 km depth (layer 6), the pattern seen in layer 5 has changed and no longer parallels the subsurface strike of the SAF.

Discussion

From the tomographic inversion, a low-velocity anomaly is clearly observed between the sub-parallel NE-dipping strands of the Banning and Mission Creek faults (B–B', Figure 4) and at relatively shallow mid-crustal depths (3.2–8 km). Independent evidence that both the Banning and Mission Creek faults dip NE at moderate angles (50° to 60°) is based on seismicity (Figure 1), earthquake focal mechanisms, geologic surface mapping [*Allen*, 1957], and gravity data. If the prominent low-velocity anomaly seen in Figures 2 and 4 is indeed bounded to the SW and NE by the Banning and Mission Creek faults, then the tomographic results confirm that the currently aseismic Mission Creek fault dips at moderate angles to the

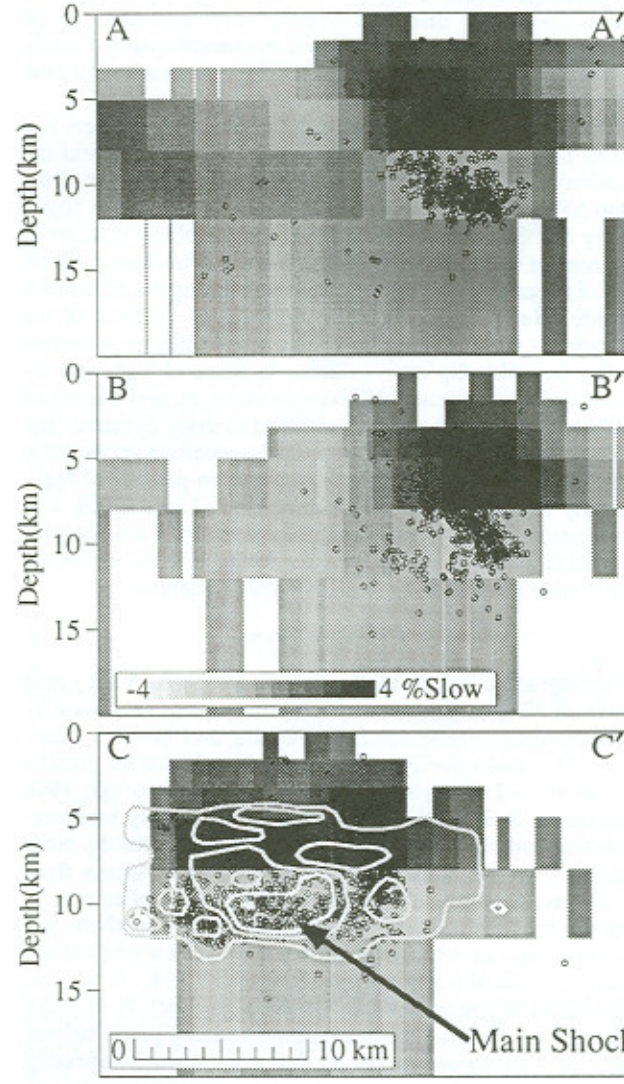

Fig. 4. Grayshade cross sections of velocity perturbations (in % slowness) relative to individual layer velocities specified in the 1-D model. Cross section orientations are shown in Figure 2a. Hypocenters projected from within 5 km to either side are shown as small open circles. In C-C', superimposed contour lines are from the projected dynamic slip distribution of the NPS mainshock [after *Hartzell*, 1989].

NE, and thus, does not merge with the Banning fault to form a single fault trace at depth.

Drill holes, gravity and seismic refraction studies indicate that basin sediments are only about 2–3 km deep in northern Coachella Valley [*e.g., Proctor,* 1968]. Thus, the low-velocity anomaly seen in layers 3 and 4 is located well into the granitic basement, and is possibly related to increased fracture density from secondary fault splays between the Banning and Mission Creek faults. Indirect evidence for such fault splays, at least in the hanging wall of the Banning fault, is provided by abundant aftershock hypocenters at depths of about 5 km, and located above the active Banning fault at depth (Figure 1). It is also interesting that both the low-velocity anomaly in layers 3 and 4, and the high-velocity anomaly in layer 5 tend to follow the strike of the deep aftershocks, rather than curve to match the observed surface fault traces. In layer 6, however, this is no longer true, suggesting that velocity perturbations below about 12 km no longer correlate with the position of the active faults at depth. One possibility is that both the Banning and Mission Creek faults are terminated by a low-angle detachment surface. Independent evidence for such a detachment (at a depth of about 10–12 km) that dips slightly north and east can be inferred from analysis of regional microearthquake activity [*Nicholson et al.,* 1986], and analysis of aftershocks from the 1986 NPS earthquake (Figure 1).

The most important observation, however, is that there is a strong correlation between high-velocity anomalies and the location of seismic strain energy release. The hypocenter of the 1986 NPS earthquake occurred between 10 and 11 km depth, nearly in the middle of the high-velocity anomaly of layer 5. The zone of maximum velocity perturbation correlates with the area of maximum dynamic slip observed during the mainshock rupture [*Hartzell,* 1989] and is surrounded by most of the aftershocks (C-C', Figure 4). This suggests that major earthquakes in strike-slip regimes occur in zones of high-velocity material that are presumably more competent, and thus more likely to sustain high stresses required to drive dynamic slip. At Parkfield and at Loma Prieta, the hypocenters of the 1966 and 1989 mainshocks similarly occurred in patches of high-velocity material [*Lees and Malin,* 1990; *Lees,* 1990]. The implication is that the tomographic inversions are imaging asperities at depth along the San Andreas fault which are responsible for producing large earthquake ruptures.

Conclusions

Tomographic images in the northern Coachella Valley near the 1986 NPS earthquake exhibit a prominent low-velocity anomaly localized between the Banning and Mission Creek faults. This low-velocity anomaly occurs well into the granitic basement, and above the primary rupture area of the 1986 mainshock. In 3-D, the outline of this low-velocity zone suggests that both the Banning and Mission Creek faults dip moderately to the NE, consistent with independent evidence from seismicity, geology and gravity studies; and implies that, at least in this area, the two major strands of the southern San Andreas fault do not merge at depth to form a single fault trace. Seismic slip during the 1986 mainshock, as well as aftershocks triggered on and off the mainshock fault plane largely occur in areas the exhibit high-velocity perturbations. The high-velocity anomalies are thus interpreted as reflecting regions of stronger, more competent material associated with asperities along the fault zone, where large earthquakes tend to initiate and areas of maximum seismic slip during dynamic ruptures tend to occur. Travel-time tomography may thus offer a means of identifying future rupture zones of earthquakes along major strike-slip faults in California.

Acknowledgments. Appreciation is extended to the Donors of the Petroleum Research Fund, ACS (C.N.) and to NSF under grant EAR 89–16543 (J.M.L.) for partial support of this work. We thank Robert Wesson, John Coakley, Gonzalo Mendoza and Chris Dietal of the USGS for their assistance in the field. Additional help with the portable digital data and acquisition of arrival times from the regional network was provided by Jack Boatwright, Doug Given and Lucy Jones.

References

Allen, C.R., San Andreas fault zone in San Gorgonio Pass, southern California, *Geol. Soc. Am. Bull.,* **68,** 315–350, 1957.

Green, S.M., Seismotectonic study of the San Andreas, Mission Creek, and Banning fault system, *M.S. Thesis,* University of California, Los Angeles, 1983.

Hartzell, S., Comparison of waveform inversion results for the rupture history of a finite fault: Application to the 1986 North Palm Springs, California, earthquake, 1989, *J. Geophys. Res.,* **94,** 7515–7534, 1989.

Jones, L.M., K.L. Hutton, D.D. Given, and C.R. Allen, The North Palm Springs, California, earthquake sequence of July 1986, *Bull. Seism. Soc. Am.,* **76,** 1828–1843, 1986.

Lahr, J.C., HYPOELLIPSE 2.0: A computer program for determining local earthquake hypocentral parameters, magnitudes and first-motion patterns, *U.S. Geol. Surv. Open–file Report 89–116,* 93 pp., 1989.

Lees, J.M., Tomographic P-wave velocity images of the Loma Prieta Earthquake Asperity, *Geophys. Res. Lett.,* **17,** 1433–1436, 1990.

Lees, J.M. and R.S. Crosson, Tomographic inversion for 3-D velocity structure at Mount St. Helens using earthquake data, *J. Geophys. Res.,* **94,** 5716–5728, 1989.

Lees, J.M. and P.E. Malin, Tomographic images of P-wave velocity variations at Parkfield, California, *J. Geophys. Res.,* **95,** 21,793–21,804, 1990.

Matti, J.C., D.M. Morton, and B.F. Cox, Distribution and geologic relations of fault systems in the vicinity of the central Transverse Ranges, southern California, *U.S. Geol. Surv. Open-File Rep. 85–365,* 23 pp., 1985.

Nicholson, C., L. Seeber, P.L. Williams, and L.R. Sykes, Seismicity and fault kinematics through the Eastern Transverse Ranges, California: Block rotation, strike-slip faulting and shallow-angle thrusts, *J. Geophys. Res.,* **91,** 4891–4908, 1986.

Proctor, R.J., Geology of the Desert Hot Springs – upper Coachella Valley area, California, *Calif. Div. of Mines and Geol. Spec. Rep. 94,* 50 pp., 1968.

J.M. Lees, Department of Geology and Geophysics, Yale University, New Haven, CT 06511-8130.

C. Nicholson, Institute for Crustal Studies, University of California, Santa Barbara, CA 93106-1100.

(Received June 18, 1991;
revised October 30, 1991;
accepted November 22, 1991)